



PREDICTION OF SUPERSONIC JET NOISE FROM A STATISTICAL ACOUSTIC MODEL AND A COMPRESSIBLE TURBULENCE CLOSURE

C. BAILLY[†] AND S. CANDEL

*Laboratoire E.M2.C. du CNRS et de l'Ecole Centrale Paris, Grande Voie des Vignes,
92295 Châtenay-Malabry Cedex, France*

AND

P. LAFON

*Direction des Etudes et Recherches d'Electricité de France, 1 avenue du Général de Gaulle,
92141 Clamart Cedex, France*

(Received 23 April 1995, and in final form 20 November 1995)

Acoustic radiation of shock free supersonic jets is modified in comparison with subsonic jet noise because of Mach wave emission. Intense noise is radiated when turbulent structures are convected supersonically relative to the ambient sound speed. Using the framework of Lighthill's equation, Ffowcs Williams and Maidanik developed an approximation of Lighthill's term for a supersonically convected acoustic source in a turbulent shear layer. From this result, a model can be deduced for axisymmetric jets. One then shows that the local knowledge of the mean flow and a characteristic time of turbulence in the source volume may be used to calculate the spectral directivity of Mach wave noise. As a consequence of this local formulation of the acoustic source term, the noise model contains a single unknown multiplicative constant. It also requires a calculation of the mean flow which may be carried out with a $k - \epsilon$ compressible turbulence model. Two cold jet cases at $M = 1.7$ and $M = 2.0$ and a hot jet at $M = 2.0$ and $T_j/T_0 = 2.5$ are analyzed. Comparisons with available experimental data and Tam's calculations based on an alternative description in terms of instability waves travelling at the convection speed show a good agreement between calculations and measurements.

© 1996 Academic Press Limited

1. INTRODUCTION

For high speed imperfectly expanded jets one can essentially identify three mechanisms of noise: turbulent mixing noise, broadband shock associated noise and screech tone. In the case of perfectly expanded jets considered here the last two components of supersonic jet noise do not require further consideration. At least two approaches may be used to predict mixing noise of high speed jets, when turbulent structures are convected supersonically relative to the ambient speed sound. The first method developed by Tam and colleagues [1, 2] is based on a stochastic instability wave model (see Figure 1). From measurements of mean flow parameters, an analytical representation of the mean flow is constructed as a starting point of the instability wave model. A method of matched asymptotic expansion then yields a solution which is valid in the far field. One single multiplicative constant is necessary with the stochastic instability wave model. It is chosen

[†]Present address: Laboratoire de Mécanique des Fluides et d'Acoustique, URA CNRS 263, Ecole Centrale de Lyon, B.P. 163, 69131 Ecully Cedex, France.

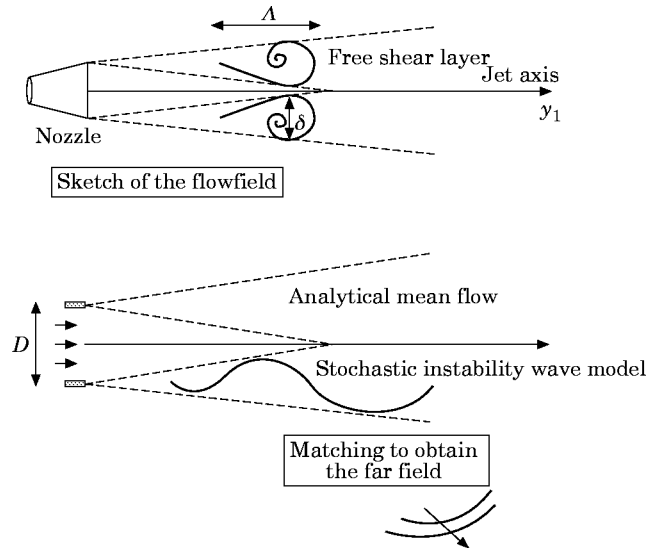


Figure 1. Tam's approach to calculate supersonic jet noise.

for best overall comparison with the experimental data of Seiner *et al.* [3]. In what follows the numerical prediction of Tam [1] will be used to compare them with the present model. Whilst this approach is valuable it also raises difficult theoretical questions. For example it is assumed that the instability modes may be obtained by taking as the velocity profile that of the mean flow. This is an important simplification of the real situation.

An alternative approach may be used to predict supersonic jet noise. Ffowcs Williams and Maidanik [4] derived an expression for acoustic sources convected supersonically in a turbulent shear layer. In their expression the acoustic autocorrelation pressure in the far field is directly associated to the space-time pressure correlation in the near field. But for Mach wave emission, experimental observations [5–8] show that the space-time correlation function takes a simple form featuring local shear flow parameters such as the convection velocity and the displacement thickness. Following this second approach one may estimate local acoustic source terms which are supersonically convected from a calculation of the mean flow using a compressible turbulence closure. An estimation of the space-time correlation pressure combined with the free space Green function of Lighthill's equation then leads to an expression of the acoustic spectral directivity. As in the first treatment of Mach wave radiation, one uses only information about the local mean flow and two turbulent quantities which are the kinetic energy k and the rate of dissipation ϵ , to represent the supersonically convected source term. Furthermore one single multiplicative constant is used in our model for all jet configurations. The present numerical results are compared with on one hand, experimental data of Tanna [9, 10] and Seiner *et al.* [3] for shock free supersonic jets up to a Mach number of 2 and a temperature ratio $T_0/T_j = 2.5$, and on other hand, with the work of Tam and Chen [1] based on Tam's instability wave model.

Section 2 summarizes some results of Lighthill's aerodynamic noise theory. The Mach wave sources are then formulated to derive the power spectral density of the radiated pressure (section 3). Section 4 compares numerical results predicted by a $k - \epsilon$ compressible code to available experimental data. Finally our acoustic model is applied to shock-free supersonic jets in a last section and comparisons between available

measurements and numerical results are carried out. The compressible code is briefly described in Appendix C.

2. Lighthill's THEORY OF AERODYNAMIC NOISE

Lighthill's theory [11, 12] constitutes one of the important contributions to the study of aerodynamic noise generation by turbulent flows. The theory relies on an inhomogeneous wave equation derived from the fundamental balance relations describing fluid motion,

$$\partial^2 \rho / \partial t^2 - c_0^2 \partial^2 \rho / \partial x_i \partial x_i = \partial^2 T_{ij} / \partial x_i \partial x_j, \quad (1)$$

where c_0 is the constant speed of sound in the ambient medium. It is assumed that the medium external to the flow is homogeneous and at rest. Lighthill's tensor appearing in the right hand side of equation (1) is $T_{ij} = \rho u_i u_j + (p - c_0^2 \rho) \delta_{ij} - \tau_{ij}$ where ρ , p , \mathbf{u} and $\boldsymbol{\tau}$ are respectively the density, the pressure, the velocity and the viscous stress tensor. Noting that acoustic waves in a homogeneous medium at rest are governed by $\partial_{ii}^2 \rho - c_0^2 \nabla^2 \rho = 0$ and using an analogy, the acoustic source term may be identified when $\partial_{ii}^2 \rho$ is not balanced by $c_0^2 \nabla^2 \rho$. One of Lighthill's results is that the source of sound is the double divergence of the T_{ij} tensor. The free space solution of equation (1) is easily expressed as

$$(\rho - \rho_0)(\mathbf{x}, t) = \rho'(\mathbf{x}, t) = \frac{\partial^2 T_{ij}}{\partial x_i \partial x_j} * \frac{1}{4\pi c_0^2 x} \delta\left(t - \frac{x}{c_0}\right) = \frac{1}{4\pi c_0^4 x} \int_V \frac{\partial^2}{\partial y_i \partial y_j} T_{ij}\left(\mathbf{y}, t - \frac{r}{c_0}\right) \frac{d\mathbf{y}}{r} \quad (2)$$

where $\mathbf{r} = \mathbf{x} - \mathbf{y}$ is the vector joining the source point \mathbf{y} in the flow volume V to the observation point \mathbf{x} and $*$ is the convolution product. The integral solution (2) has an asymptotic form for large r ,

$$\rho'(\mathbf{x}, t) \sim \frac{1}{4\pi c_0^4 x} \frac{x_i x_j}{x^2} \int_V \frac{\partial^2}{\partial t^2} T_{ij}\left(\mathbf{y}, t - \frac{r}{c_0}\right) d\mathbf{y} \quad (3)$$

where the symbol \sim means is equal to for large r . The far field noise is then deduced from the autocorrelation function

$$C_{pp}(\mathbf{x}, \tau) = \frac{\overline{\rho'(\mathbf{x}, t)\rho'(\mathbf{x}, t + \tau)}}{\rho_0 c_0^{-3}} = \frac{1}{\rho_0 c_0^{-3}} \lim_{T \rightarrow \infty} \frac{1}{2T} \int_{-T}^T \rho'(\mathbf{x}, t)\rho'(\mathbf{x}, t + \tau) dt. \quad (4)$$

The acoustic intensity $I(\mathbf{x})$ is directly deduced from this expression by setting $\tau = 0$: $I(\mathbf{x}) = C_{pp}(\mathbf{x}, \tau = 0)$.

Furthermore, the power spectral density $S_{pp}(\mathbf{x}, \omega)$ where ω is the angular frequency in the fixed frame of the observation point \mathbf{x} is defined as

$$S_{pp}(\mathbf{x}, \omega) = \frac{1}{2\pi} \int_{-\infty}^{\infty} C_{pp}(\mathbf{x}, \tau) e^{i\omega\tau} d\tau \quad (5)$$

The far field correlation function of the pressure expressed for stationary turbulence [13, 14] takes the form

$$C_{pp}(\mathbf{x}, \tau) \sim \frac{1}{16\pi^2 \rho_0 c_0^5 x^2} \frac{\partial^4}{\partial \tau^4} \iint_V \overline{T_{ij}(\mathbf{y}, t) T_{kl}\left(\mathbf{y} + \boldsymbol{\eta}, t + \tau - \frac{\mathbf{x} \cdot \boldsymbol{\eta}}{x c_0}\right)} d\mathbf{y} d\boldsymbol{\eta}, \quad (6)$$

where $\mathbf{x} \cdot \boldsymbol{\eta}/xc_0$ is the time separation in the observer frame between signals emitted simultaneously by two sources points \mathbf{y} and $\mathbf{y} + \boldsymbol{\eta}$. The description of source convection may be improved by introducing a reference frame moving at convection speed U_c . Defining $\boldsymbol{\xi} = \boldsymbol{\eta} - U_c \tau \mathbf{y}_1$, Ffowcs Williams [13] showed that

$$C_{pp}(\mathbf{x}, \tau) \sim \frac{1}{16\pi^2 \rho_0 c_0^5 x^2} \int \frac{1}{C^5} \frac{\partial^4}{\partial \tau^4} \int_V \overline{T_{ij}(\mathbf{y}, t) T_{kl} \left(\mathbf{y} + \boldsymbol{\xi}, t + \tau - \frac{\mathbf{x} \cdot \boldsymbol{\xi}}{xc_0} \right)} d\xi d\mathbf{y}, \quad (7)$$

where C is a Doppler or convection factor [13, 15]:

$$C = C(\mathbf{x}, \mathbf{y}) = [(1 - M_c \cos \theta)^2 + (\omega_r L / \sqrt{\pi} U_c)^2]^{1/2}, \quad \cos \theta = (x_1 - y_1) / |\mathbf{x} - \mathbf{y}|. \quad (8)$$

In these expressions, $M_c = M_c(\mathbf{y}) = U_c/c_0$ is the convection Mach number, $\omega_r = \omega_r(\mathbf{y})$ is a characteristic angular frequency of turbulence and $L = L(\mathbf{y})$ is an integral length of turbulence. According to this expression the Doppler factor resulting from the change of frame does not vanish at the Mach angle $\theta^* = \cos^{-1}(1/M_c)$ as in the radiation problem of a single point moving source.

At this step, expression (7) is an implicit integral solution. However, in assuming on the one hand isentropic fluctuations $dp = c^2 d\rho$ and an isothermal $dp = c_0^2 d\rho$, and on the other hand approximating the Reynolds stress tensor $\rho u_i u_j$ by $\rho_r u_i u_j$ where ρ_r designates the turbulent fluctuations of density, an explicit solution for the density can be obtained. In the case of subsonic jet noise, the distance over which the turbulence is coherent is short compared to an acoustic wavelength in the moving frame and the retarded time can be neglected in the integral expression (7). This result may be used, as exemplified in many studies, to estimate the acoustic radiation of subsonic and weakly supersonic free jets corresponding to subsonic convection Mach numbers, see references [15–21] for analytic developments, references [22–24] for recent numerical calculations and [25] for an application to coaxial jets.

3. POWER SPECTRAL DENSITY OF MACH WAVE NOISE

In the case of supersonic jet noise, the retarded time appearing in equation (7) must be retained, and the approximation of the Reynolds stress tensor by $\rho_r u_i u_j$ is invalid. Phillips [26] first studied Mach wave radiation of a supersonic shear flow. In his analysis, Lighthill's equation was replaced by a convected wave equation where a part of the mean flow effects were included in the wave operator rather than in the source term. This equation led to an interesting acoustic analogy in a sense that only the velocity field appeared in the source term. A description of an asymptotic acoustic field was derived for large Mach numbers by assuming a known turbulent velocity field. Early experiments, on Mach wave radiation were carried out by Laufer [26] for a supersonic turbulent boundary layer. The Green function of Phillips' is now known in the case of a plug flow [27]. An exact wave equation for acoustic fluctuations radiated in a shear flow was derived by Lilley [28, 29].

Another point of view was developed by Ffowcs, Williams and Maidanik [4] starting from Lighthill's equation (1) combined with an exact reformulation of the flow equations. The aim of their analysis was to relate the Mach wave field to specific turbulent properties in this particular case. The calculation begins with the exact free space integral solution (2)

of Lighthill's equation. Noting that the convolution product $\partial_{ij} * g = f * \partial_{ij}g$, the integral solution in the far field may be written as

$$\begin{aligned} \rho'(x, t) &= \frac{\partial T_{ij}}{\partial x_i} * \frac{\partial}{\partial x_j} \left[\frac{1}{4\pi c_0^2 x} \delta\left(t - \frac{x}{c_0}\right) \right] \sim \frac{\partial T_{ij}}{\partial x_i} * \left\{ -\frac{x_j}{x c_0} \frac{1}{4\pi c_0^2 x} \delta\left(t - \frac{x}{c_0}\right) \right\} \\ &\sim \frac{\partial^2 T_{ij}}{\partial t \partial x_i} * \left\{ -\frac{x_j}{x c_0} \frac{1}{4\pi c_0^2 x} \delta\left(t - \frac{x}{c_0}\right) \right\} \end{aligned} \quad (9)$$

Hence

$$\rho'(\mathbf{x}, t) \sim -\frac{1}{4\pi c_0^3} \int_V \frac{r_j}{r} \frac{\partial^2 T_{ij}}{\partial t \partial y_i}(\mathbf{y}, t) \delta\left(t - \frac{r}{c_0}\right) \frac{d\mathbf{y}}{r} \sim -\frac{1}{4\pi c_0^3} \int_V \frac{\partial^2 T_{ir}}{\partial t \partial y_i}(\mathbf{y}, t - \frac{r}{c_0}) \frac{d\mathbf{y}}{r}, \quad (10)$$

where one here uses the projection of Lighthill's tensor in the observation direction \mathbf{r} . The previous integrand may be written more explicitly by making use of the momentum conservation equations,

$$\partial(\rho u_j)/\partial t + \partial(\rho u_i u_j)/\partial y_i = -\partial p/\partial y_i + \partial \tau_{ij}/\partial y_i,$$

projected in the direction r :

$$(\partial/\partial y_i)[\rho u_i u_r + p \delta_{ir} - \tau_{ir}] = -\partial(\rho u_r)/\partial t.$$

Then

$$\frac{1}{c_0} \frac{\partial^2 T_{ri}}{\partial t \partial y_i} = \frac{1}{c_0} \frac{\partial^2}{\partial t \partial y_i} [\rho u_i u_r + (p - c_0^2 \rho) \delta_{ir} - \tau_{ir}] + \frac{1}{c_0} \frac{\partial}{\partial t} \left\{ \frac{\partial(\rho u_r)}{\partial t} + c_0^2 \frac{\partial \rho}{\partial y_r} \right\}. \quad (11)$$

It is known that the two source strengths $-(1/c_0)\partial f/\partial t$ and $\partial f/\partial y_r$ lead to the same acoustic far field. This is clearly shown by the two integral solutions (3) and (10). One may then replace the temporal derivative of ρu_r by a spatial derivation. The equivalent source term for the acoustic far field then becomes

$$\frac{1}{c_0} \frac{\partial^2 T_{ri}}{\partial t \partial y_i} \sim \frac{\partial^2}{\partial t \partial y_r} [\rho(u_r - c_0)]. \quad (12)$$

Upon inserting a decomposition of the velocity field in terms of a mean component U_i and a fluctuation u_i such that $\mathbf{u} = \mathbf{U} + \mathbf{u}$, expression (12) becomes:

$$\frac{1}{c_0} \frac{\partial^2 T_{ri}}{\partial t \partial y_i} \sim (U_r - c_0) \underbrace{\frac{\partial^2 \rho}{\partial t \partial y_r}}_{\textcircled{1}} + \underbrace{\frac{\partial \rho}{\partial t} \frac{\partial U_r}{\partial y_r}}_{\textcircled{2}} + \underbrace{\frac{\partial^2(\rho u_r)}{\partial t \partial y_r}}_{\textcircled{3}}. \quad (13)$$

Considering directions close to the Mach angle $\theta^* = \cos^{-1}(1/M_c)$ (see Figure 2), one may assume that $1 - M_c \cos \theta \equiv 0$. The first term of equation (13) vanishes and only the last two terms must be considered. Estimates of these terms may be deduced from the characteristic variables of the flow, Λ a typical scale of large structures, δ the mixing layer

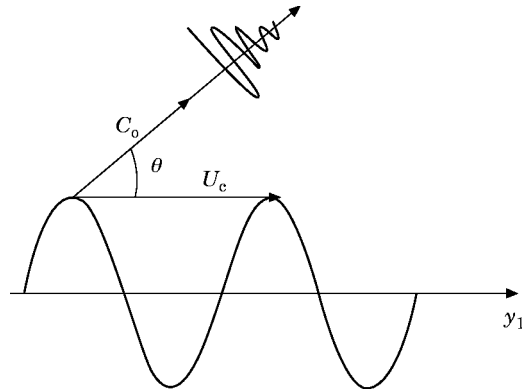


Figure 2. Mach wave radiation from perturbations convected at a supersonic speed.

thickness, U a characteristic velocity of the mean flow, ρ a characteristic density fluctuation and τ a characteristic turbulence scale:

$$\left\{ \begin{array}{l} \textcircled{2} \quad \frac{\partial \rho}{\partial t} \frac{\partial U_r}{\partial y_r} \sim \frac{\rho}{\tau} \frac{U}{\delta} \\ \textcircled{3} \quad \frac{\partial^2 (\rho u_r)}{\partial t \partial y_r} \sim \frac{\rho}{\tau} \frac{u'}{A} \end{array} \right\},$$

and the ratio of the two terms is equal to

$$\frac{\textcircled{2}}{\textcircled{3}} \sim \frac{U}{u'} \frac{A}{\delta}.$$

For compressible mixing layer turbulence [30, 31], $(u'/U)_{\max} \simeq 15\%$, and $A \geq \delta$. In a first approximation, only the second term of equation (13) should be retained,

$$\frac{1}{c_0} \frac{\partial^2 T_{ri}}{\partial t \partial y_i} \sim \frac{\partial \rho}{\partial t} \frac{\partial U_r}{\partial y_r} \sim \frac{1}{c^2} \frac{\partial p}{\partial t} \frac{\partial U_r}{\partial y_r}, \quad (14)$$

where the last evaluation is obtained by considering that the fluctuations are locally isentropic. The far field sound pressure features a term amplified linearly by the mean flow gradient,

$$\rho'(\mathbf{x}, t) \sim -\frac{1}{4\pi c_0^2} \int_{V^*} \left[\frac{1}{c^2} \frac{\partial p}{\partial t} \frac{\partial U_r}{\partial y_r} \right] \left(\mathbf{y}, t - \frac{r}{c_0} \right) \frac{d\mathbf{y}}{r} \quad (15)$$

where $\partial U_r / \partial y_r = (r_i r_j / r^2) \partial U_i / \partial y_j$. The integration is performed over the source volume V^* defined as the set of points in the flow for which the convection Mach number exceeds unity $V^* = \{\mathbf{y}, M_c(\mathbf{y}) \geq 1\}$.

At this point it is worth discussing expression (15). Indeed it has been pointed out previously that it may not be valid to express the acoustic far field as a function of linear source terms. It has been implied by Crow [32] and Ffowcs Williams [33] that such terms may introduce secular effects in the solution. It is known that such terms are responsible for refraction effects and this has motivated the analysis of Doak [29] and Lilley [28] and their proposed modification of the wave operator. In the case of Mach wave radiation which dominates the noise from high speed jets this criticism is of lesser importance because the acoustic far field is similar to the near field pressure fluctuations. The dominant effect

is the convection of turbulent fluctuations in the shear flow. This is well demonstrated in the detailed experiments of Parthasarathy and Massier [7]. Their data supports the theory of Ffowcs Williams and Maidanik justifying the linear relationship exploited in the present model.

Among the nine terms composing the local velocity gradient, the largest is $\partial U_1/\partial y_2$, since the mean flow is essentially oriented in the axial direction. Then

$$\rho'(\mathbf{x}, t) \sim -\frac{1}{4\pi c_0^2} \int_{V^*} \frac{r_1 r_2}{r^2} \left[\frac{1}{c^2} \frac{\partial p}{\partial t} \frac{\partial U_1}{\partial y_2} \right] \left(\mathbf{y}, t - \frac{r}{c_0} \right) \frac{d\mathbf{y}}{r} \quad (16)$$

The correlation function (4) may be expressed as

$$C_{pp}(\mathbf{x}, t) \sim \frac{1}{16\pi^2 c_0 \rho_0} \int \int_{V^*} \overline{f\left(\mathbf{y}, t - \frac{|\mathbf{x} - \mathbf{y}|}{c_0}\right) f\left(\mathbf{y}', t + \tau - \frac{|\mathbf{x} - \mathbf{y}'|}{c_0}\right)} d\mathbf{y} d\mathbf{y}', \quad (17)$$

where the source term f is

$$f(\mathbf{y}, t) = \frac{(x_1 - y_1)(x_2 - y_2)}{|\mathbf{x} - \mathbf{y}|^2} \left[\frac{1}{c^2} \frac{\partial U_1}{\partial y_2} \frac{\partial p}{\partial t} \right] (\mathbf{y}, t).$$

One assumes that the local sound speed and the local mean flow gradient are constant over the correlation volume of turbulence. With the notation $\cos \theta = (x_1 - y_1)/|\mathbf{x} - \mathbf{y}|$, $\sin \theta = (x_2 - y_2)/|\mathbf{x} - \mathbf{y}|$, $\boldsymbol{\eta} = \mathbf{y}' - \mathbf{y}$, the cross-correlation (17) becomes:

$$C_{pp}(\mathbf{x}, \tau) \sim \frac{1}{16\pi^2 c_0 \rho_0} \int_{V^*} \cos^2 \theta \sin^2 \theta \left(\frac{1}{c^2} \frac{\partial U_1}{\partial y_2} \right)^2 \left\{ \int_{V^*} \overline{\frac{\partial p'}{\partial t} \frac{\partial p''}{\partial t}} d\boldsymbol{\eta} \right\} d\mathbf{y}, \quad (18)$$

where the superscripts ' and '' respectively designate values at the source points:

$$(\mathbf{y}, t - |\mathbf{x} - \mathbf{y}|/c_0) \text{ and } (\mathbf{y} + \boldsymbol{\eta}, t - |\mathbf{x} - \mathbf{y} - \boldsymbol{\eta}|/c_0).$$

For a stationary turbulence an integration by parts shows (see Appendix A) the correlation function of the pressure time derivative may be calculated as the second derivative of the pressure correlation:

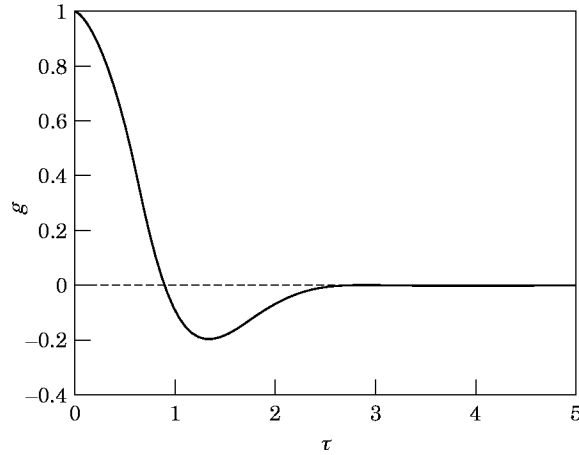
$$\overline{\frac{\partial p'}{\partial t} \frac{\partial p''}{\partial t}} = -\frac{\partial^2}{\partial \tau^2} \overline{p' p''}.$$

To model the correlation $\overline{p' p''}$ one may use the data of Parthasarathy *et al.* [7, 8]. It has been found that this correlation has a form very close to the following function g :

$$\overline{p' p''}(\boldsymbol{\eta}, \tau) = \overline{p' p''}(\boldsymbol{\eta}, 0) g(\tau) \text{ with } g(\tau) = [1 - \frac{5}{4} \omega_i^2 \tau^2] e^{-\omega_i^2 \tau^2}. \quad (19)$$

The function g is plotted in Figure 3 and some of its properties are given in Appendix B. The first integration over the correlation volume of turbulence was proposed by Ffowcs Williams [13]:

$$\int_{V^*} \overline{\frac{\partial p'}{\partial t} \frac{\partial p''}{\partial t}} d\boldsymbol{\eta} \Big|_{\tau=0} = \left(\frac{\partial p}{\partial t} \right)^2 c_0 \tau_i \xi_s, \quad (20)$$

Figure 3. Time correlation function g of the pressure ($\omega_t = 1$).

where τ_t is the lifetime of turbulence and ξ_s is the correlation area perpendicular to the Mach wave direction θ^* . The mean square value of the time derivative of the pressure was estimated by Kistler and Chen [5] for a supersonic turbulent boundary layer as

$$\overline{\left(\frac{\partial p}{\partial t}\right)^2} \simeq \frac{1}{2} \frac{c_0^2 M_c^2}{\delta_1^2} p_0^2, \quad (21)$$

where δ_1 is the boundary layer thickness. The same expression may be used in the present context by taking for δ_1 the half-width of the jet, defined as

$$\delta_1 = \int_{y_2=0}^{y_2^*} \left(1 - \frac{U_1}{U_1(y_2=0)}\right) dy_2, \quad (22)$$

in which y_2^* is the radial location where the velocity U equals $0.01 U_1(y_2=0)$. On the other hand, from the previous expression of the term $\overline{p'p''}$, the integration over the correlation volume in expression (18) may be expressed as

$$\int_{V^*} \frac{\partial p'}{\partial t} \frac{\partial p''}{\partial t} d\mathbf{\eta} = -\frac{\partial^2 g}{\partial \tau^2} \int_{V^*} \overline{p'p''}(\mathbf{\eta}, 0) d\mathbf{\eta}. \quad (23)$$

Thus, by identification with equation (20) for $\tau = 0$, one finds that

$$\omega_t^2 = \frac{2}{9} \frac{U_c^2}{\delta_1^2} \text{ and } \int_{V^*} \overline{p'p''}(\mathbf{\eta}, 0) d\mathbf{\eta} = \frac{p_0^2}{2} c_0 \tau_t \xi_s. \quad (24)$$

The correlation area ξ_s can be related to the displacement thickness [9] by

$$\xi_s \simeq \delta_1^2 / \cos^2 \theta \simeq \delta_1^2 M_c. \quad (25)$$

Hence, the expression for the far field autocorrelation pressure is

$$C_{pp}(x, \tau) \sim \frac{p_0^2}{32\pi^2 \rho_0} \int_{V^*} \cos^2 \theta \sin^2 \theta \left(\frac{1}{c^2} \frac{\partial U_1}{\partial y_2}\right)^2 \left(-\frac{d^2 g}{d\tau^2}\right) \tau_t \delta_1^2 M_c dy, \quad (26)$$

In these expressions, one assumes that the observer point \mathbf{x} is in the direction of Mach waves, and so that all the radiated energy is concentrated in this direction. The acoustic field in other directions is deduced by multiplying the intensity in the Mach wave direction by the normalized convection factor (8):

$$\tilde{C}^{-5} = [\alpha^2 M_c^2 / ((1 - M_c \cos \theta)^2 + \alpha^2 M_c^2)]^{5/2}. \quad (27)$$

The acoustic intensity in the far field is then obtained by writing the previous expression for $\tau = 0$, with $-\mathrm{d}^2 g / \mathrm{d}\tau^2|_{\tau=0} = \frac{9}{2} \omega_t^2 = U_c^2 / \delta_1^2$. The acoustic intensity becomes

$$I(\mathbf{x}) \sim \frac{p_0^2 c_0^2}{32\pi^2 \rho_0} \int_{V^*} \frac{\cos^2 \theta \sin^2 \theta}{\tilde{C}^5} \left(\frac{1}{c^2} \frac{\partial U_1}{\partial y_2} \right)^2 \tau_t M_c^3 \mathrm{d}\mathbf{y}. \quad (28)$$

As indicated in the previous section, the power spectral density S_{pp} may be obtained by taking the Fourier transform of the autocorrelation function: i.e.,

$$S_{pp}(\mathbf{x}, \omega) \sim \frac{p_0^2}{32\pi^2 \rho_0} \int_{V^*} \frac{\cos^2 \theta \sin^2 \theta}{\tilde{C}^5} \omega^2 G(\omega) \tau_t \delta_1^2 M_c \mathrm{d}\mathbf{y}, \quad (29)$$

where G is the Fourier transform of g (see Appendix B):

$$G(\omega) = \left[1 - \frac{5}{8} \left(1 - \frac{\omega^2}{2\omega_t^2} \right) \right] \frac{1}{2\sqrt{\pi}\omega_t} e^{-\omega^2/4\omega_t^2}. \quad (30)$$

The local knowledge of the mean flow gradient $\partial U_1(\mathbf{y}) / \partial y_2$, the speed of sound $c(\mathbf{y})$, the convection Mach number $M_c(\mathbf{y})$ and a characteristic turbulence time $\tau_t(\mathbf{y})$ allows calculations by integration of expressions (28) and (29) over the volume V^* yielding the acoustic intensity and the power spectral density due to Mach waves. All these quantities may be deduced from an aerodynamic calculation by using a turbulence closure scheme such as a compressible $k-\epsilon$ model.

4. APPLICATION TO FREE SUPERSONIC JET NOISE

Numerical calculations of the mean flow field are first described. These calculations are compared with measurements of Seiner *et al.* [3, 34]. Acoustic results are then reported. Directivity, acoustic power and efficiency, narrow band spectra are also compared with available experimental data of Laufer *et al.* [35], Tanna *et al.* [9, 10] and Seiner *et al.* [3, 34]. A sketch of the geometry is shown in Figure 4.

4.1. AERODYNAMIC RESULTS

The aerodynamic field is obtained from a numerical solution of Reynolds average Navier-Stokes equations associated with a $k-\epsilon$ closure. These calculations are carried out with an axisymmetric compressible version of the ESTET code developed by the ‘‘Laboratoire National Hydraulique’’ of the ‘‘Direction des Etudes et Recherches d’Electricit  de France’’ (see Appendix A for further information and the turbulence model equations). Compressibility effects are accounted for by introducing an energy dissipation resulting from dilatation processes into the standard $k-\epsilon$ model (see reference [36] for instance). Computations were carried out for unheated free jets at nominal Mach numbers of 1.67 and 2 and for a hot jet at $M = 2$. Nominal flow parameters are gathered in Table 1. The ambient, the nominal jet and stagnation temperatures are respectively designated as T_0 , T_j and T_t . Numerical results are compared with the recent experimental data of Seiner *et al.* [3, 34].

TABLE 1
Mean flow data

M	$T_i(K)$	$T_j(K)$	γ	U_j/c_0	T_j/T_0	$c_j(ms^{-1})$	
1.67	464	298	1.40	1.67	1.0	346	cold jet
2.0	536	298	1.40	2.0	1.0	346	cold jet
2.0	1370	761	1.36	3.3	2.5	545	hot jet

Figure 5(a) displays Mach number contour plots and spatial distributions of the turbulent kinetic energy per unit mass k for the case of a hot jet at $M = 2$. The computational domain has $20D$ in the axial direction, with a nozzle diameter D of 0.025 m. The jet mixing layers corresponding to the maximum of turbulent energy k may be identified in Figure 5(b). Production of kinetic energy k is directly associated with velocity gradients, which reach a maximum in the mixing layers and are negligible in the potential core. The length of this potential core X_c , defined as the length where the mean center-line velocity is less or equal to $0.99 U_j$, increases with the Mach number while the lateral mixing layers become thinner. Figure 6 demonstrates the close agreement between predicted and measured mean center-line velocity for the two jets with a nominal Mach number of 2. For the hot jet case at $M = 2$, the predicted length of the potential core, $X_c \approx 9.3 D$, is slightly smaller than the value measured by Seiner *et al.* [3]. The faster decrease of the mean center-line velocity with increasing jet temperature observed experimentally by Seiner *et al.* [3] is retrieved in the present calculation. The small wiggles observed for the hot jet are due to a slight mismatch between the jet exhaust pressure and the ambient pressure. Comparison of predicted velocity profiles with experimental data for several axial locations are reported in Figure 7. These profiles collapse on the fitted curve given by Seiner *et al.* [34]. In Figure 8 comparisons between the calculated radius to half velocity, defined as the radial location where the mean velocity U_1 is equal to $0.5U_1(y_2 = 0)$, and available measurements [3] is shown for the cold jet at $M = 2.0$. Comparison of velocity profiles with experimental data of reference [34] for different axial locations are reported in Figure 8. All these comparisons indicate that suitable numerical predictions are obtained for the axial velocity profile and the jet spreading rate.

The self-similar behavior of radial profiles of turbulence intensity σ defined as $\sigma = \sqrt{u_{t_i}^2}/U_1(y_2 = 0)$ were investigated for different axial locations and plotted in Figure 9. The maximum of fluctuations is $\sigma \approx 11\%$ and is reached for $\eta \approx -0.1$ (see Figure 9 for

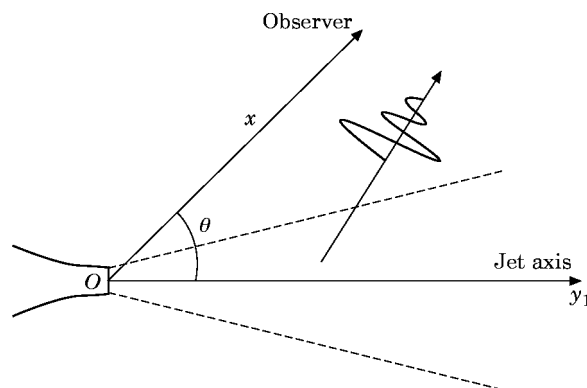


Figure 4. Geometry of the problem.

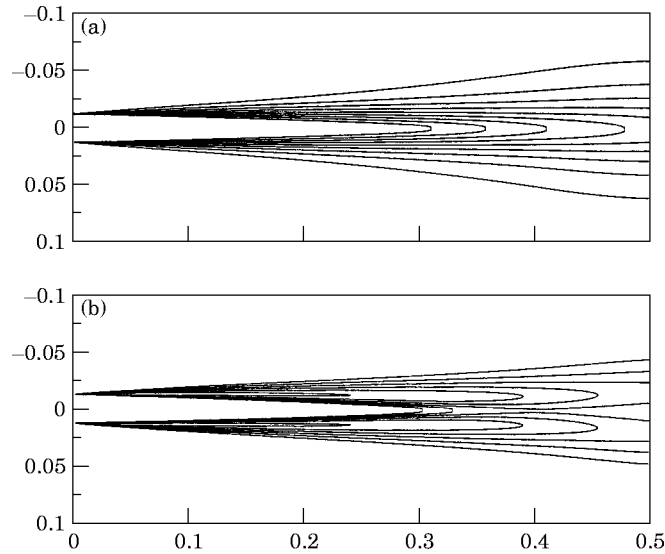


Figure 5. Hot jet at Mach 2.0 (a) Mach number contour plot showing six isolines from 0.0 to 1.8 with a step of 0.2; (b) turbulent kinetic energy contour plot showing nine isolines from 3500 m² s⁻² to 12 500 m² s⁻² with a step of 1125 m² s⁻².

the definition of η) which corresponds to a maximum of turbulence intensity located in $y_2 \simeq D/2$. This level of turbulence intensity is probably under-estimated due to the $k-\epsilon$ closure, which assumes a nearly isotropic turbulence. Indeed the concept of turbulent viscosity (see Appendix C) cannot correctly represent the splitting of the kinetic energy between the longitudinal and transversal directions. Several authors [30, 31] showed that in the case of a compressible turbulence the maximum expected value for σ is of the order of 15%. Figure 10 displays the axial evolution of the fluctuation Mach number M_t defined as $M_t = \sqrt{k}/2c$ as a function of the normalized axial direction y_1/X_c where X_c is the length of the potential core. The fluctuation Mach number rises with y_1/X_c , reaches

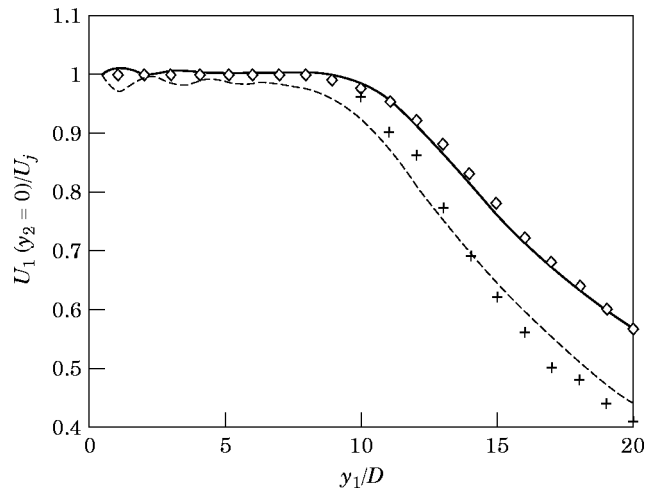


Figure 6. Jet at $M = 2$. Predicted mean axial velocity. Calculations: —, $T_j/T_0 = 1$; ---, $T_j/T_0 = 2.5$. Measurements of Seiner *et al.* [3]: \diamond , $T_j/T_0 = 1$; +, $T_j/T_0 = 2.5$.

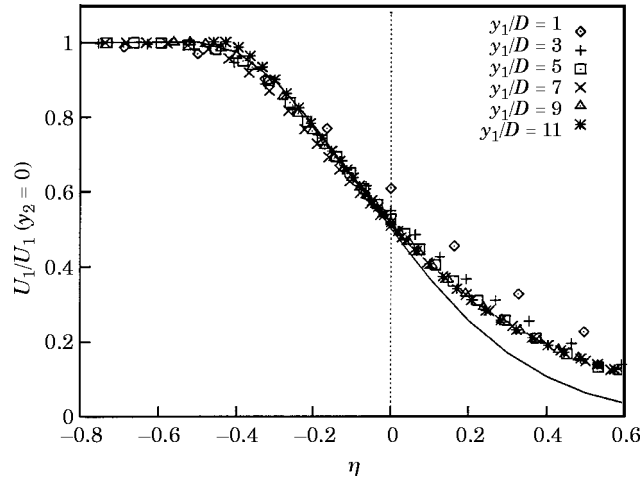


Figure 7. Jet at $M = 2$ and $T_j/T_0 = 1$. Radial velocity profiles at different locations. —, Measurements of Seiner *et al.* fitted to a half-Gaussian [34]. Symbols: predicted profiles at different axial locations. The variable η is defined as $\eta = (y_2 - y_2(0.5))/\delta$, where $y_2(0.5)$ is the radial location where the velocity equals $U_1 = 0.5U_1(y_2 = 0)$ and δ is the local shear layer thickness $\delta = y_2(0.1) - y_2(0.9)$, which represents the radial distance between the points where the local velocity is $U_1 = 0.1U_1(y_2 = 0)$ and $U_1 = 0.9U_1(y_2 = 0)$.

a maximum at about $y_1 \simeq 1.7X_c$, and then falls. Experimental observations of Lau *et al.* [30] shows similar evolutions for supersonic jets at $M = 1.37$.

4.2. ACOUSTIC RESULTS

In order to use expressions (28) and (29) to calculate the acoustic intensity and power spectral density, it is necessary to specify the convection velocity, the characteristic time or the angular frequency and an integral length scale of turbulence. The convection velocity $U_c(\mathbf{y})$ cannot be directly deduced from the present aerodynamic calculations. This velocity is estimated as $0.67U_1(y_2 = 0)$, where $U_1(y_2 = 0)$ is the mean velocity on the jet axis in the local section y_1 . As a consequence, the convection velocity is a function of the axial distance

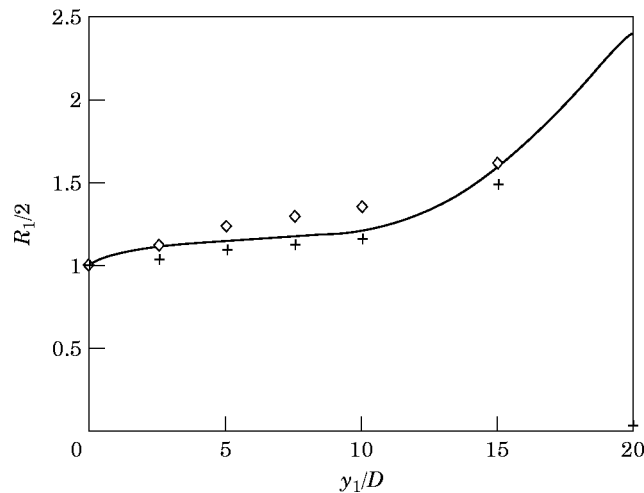


Figure 8. Jet at $M = 2$ and $T_j/T_0 = 1$. Radius to half velocity normalized by the nozzle diameter D . Calculations: —, Measurements of Seiner *et al.*: \diamond , $T_j/T_0 = 0.62$; + $T_j/T_0 = 1.51$.

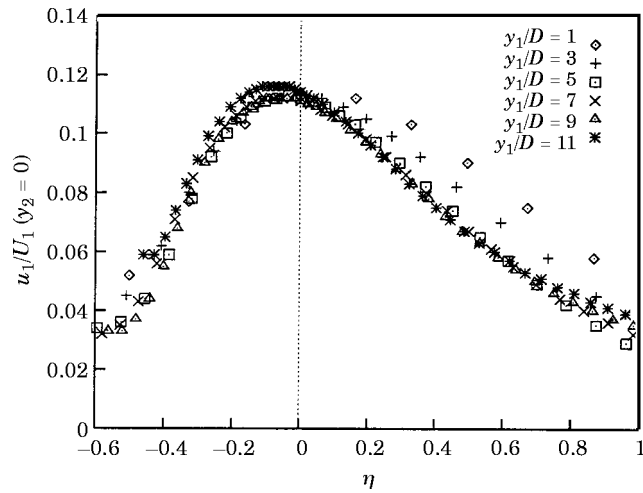


Figure 9. Jet at $M = 2$ and $T_j/T_0 = 1$. Predicted radial profiles of turbulence intensity $\sigma = \sqrt{u_i^2}/U_1(y_2 = 0)$ at different locations. See Figure 7 for the definition of η .

y_1 . The turbulence characteristic time τ_t is given by the ratio $\tau_t \sim k/\epsilon$, and the angular frequency ω_t is then obtained by $\omega_t \sim 2\pi\epsilon/k$, where k is the turbulent kinetic energy per unit mass and ϵ the dissipation rate, that is to say the rate of transfer of kinetic energy per unit mass and per unit time. For the convection factor \tilde{C} the turbulence integral scale L is estimated from the local values of k and ϵ : $L \sim k^{3/2}/\epsilon$.

The two turbulence scales τ_t and L are characteristic of the large structures. Indeed a suitable estimation of the integral length of turbulence, which can be determined by spectral considerations for an isotropic turbulence, is

$$L = \int_0^\infty f(r) dr \simeq \frac{k^{3/2}}{\epsilon}$$

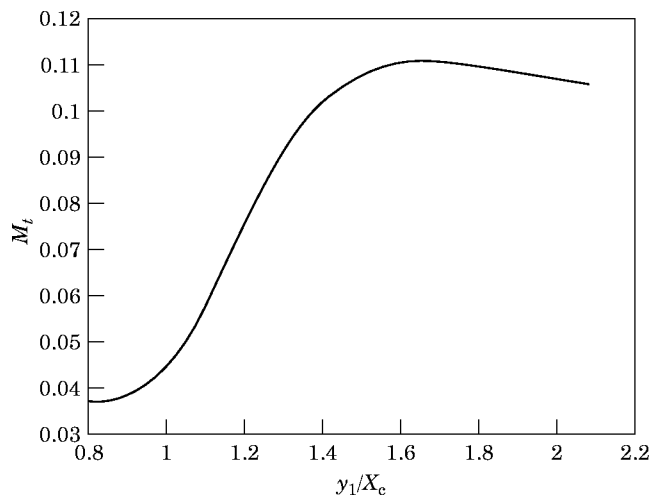


Figure 10. Jet at $M = 2$ and $T_j/T_0 = 1$. Axial profile of the fluctuation Mach number $M_t = \sqrt{k}/2c$ as a function of y_1/X_c where X_c is the length of the potential core.

where f is the von Kármán-Howarth longitudinal correlation function. This model uses quantities which depend implicitly on unknown scaling constants. An adjustable multiplicative constant is also necessary in the expression of the acoustic intensity. This single global factor β is determined by comparison with experimental data of Tanna *et al.* [9, 10] and Seiner *et al.* [3] for a jet at $M = 2$ and $T_j/T_0 = 1$, and an observation angle $\theta = 39^\circ$: $\beta \approx 1.38 \times 10^{-2}$. This point is taken as reference for all other flow configurations. Acoustic levels for directivity and narrow band spectra, are always given per unit of nozzle area and corrected to the distance x of the observer, with a reference of $I_0 = 10^{-12} \text{ Wm}^{-2}$.

4.2.1. Directivity

Figure 11 shows the calculated acoustic intensity for the two cold and hot jets at $M = 2$ and corresponding experimental data of Tanna *et al.* [9] and Seiner *et al.* [3]. The sharp directivity pattern characteristic of eddy Mach wave radiation is retrieved. The model predicts only the acoustic radiation due to Mach waves. Hence, the calculated intensity is valid for an observation angle centered around $\theta^* = \cos^{-1}(1/M_c)$. However, one sees that Mach waves dominate the acoustic radiation in the cases under investigation, and that, in particular, this partial prediction of the directivity yields a correct estimate of the acoustic power. One here observes the influence of temperature on the radiated sound field. Indeed, the variation of the mean temperature is taken into account through the factor c^4 in equation (28). In the hot jet case, the acoustic level is roughly equal to that reached in the cold jet case because of the decrease of the jet shear density, but the direction of acoustic radiation is modified. To have a complete prediction of the directivity, it is necessary to include the contribution of mixing noise [23, 24]. This has been done yielding an excellent prediction at $\theta = 90^\circ$, as may be seen in Figure 12.

The directivity of the cold jet at $M = 1.67$ is plotted in Figure 13 and compared with measurements of Tanna *et al.* [9]. One again retrieves the sharp directivity pattern from Mach waves with a good accuracy. It is again necessary to add the mixing noise component to get a correct estimation of the directivity at $\theta = 90^\circ$ and in the backwards quadrant.

In the supersonic free jet case, when the acoustic radiation is dominated by Mach waves, the acoustic power evolves according to the following dimensional law, see references [13, 14]: $W \sim (\rho_j^2/\rho_0)D^2U_j^3$. The acoustic power is thus proportional to the square of the

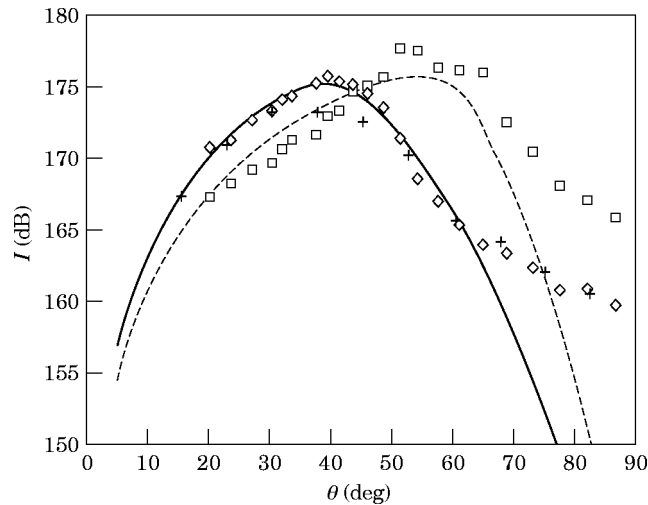


Figure 11. Jet at $M = 2$: Acoustic directivity. Calculations: —, $T_j/T_0 = 1$; ---, $T_j/T_0 = 2.5$. Measurements of Seiner *et al.* [3] \diamond , $T_j/T_0 = 1$; \square , $T_j/T_0 = 2.5$. Experimental points of Tanna *et al.* [9]: +, $T_j/T_0 = 1$.

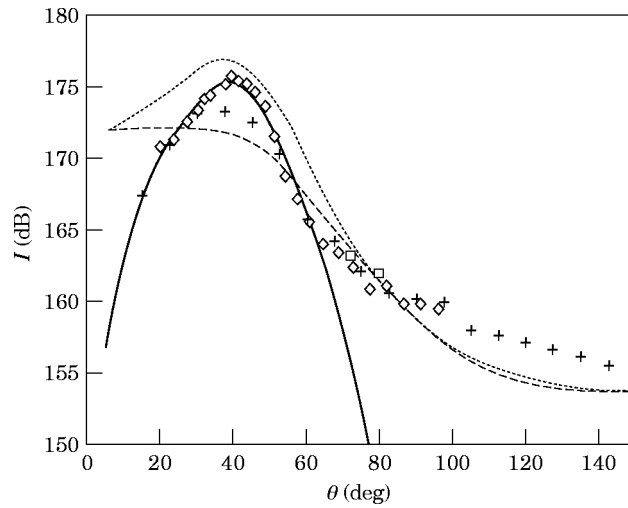


Figure 12. Jet at $M = 2$ and $T_j/T_0 = 1$. Acoustic directivity. —, Mach wave noise component; ---, mixing noise component;, sum of the two components; ◆, key for symbols as Figure 11.

density ρ_j . Also, in the hot jet case, the velocity increase is balanced by the decrease of the density. The acoustic efficiency η is another interesting quantity which may be used to characterize acoustic radiation. It is defined as the ratio between the acoustic power and the mechanical power, i.e. between the radiated energy and the supplied energy. For a round free jet, the mechanical power is given by $W_m = (\pi D^2/4)\rho_j U_j^3$.

Dimensional laws and acoustic efficiencies are given in Table 2 for free turbulent flows with subsonic or supersonic convection Mach numbers. One observes that η increases as M_c^2 when the convection Mach number is subsonic, and becomes roughly constant when the convection Mach number is supersonic. The acoustic energy radiated is then directly proportional to the energy supplied by the jet. For instance, a ratio $U_j/c_0 \sim 3.3$ in the present case leads to an acoustic efficiency η equal to 0.5%.

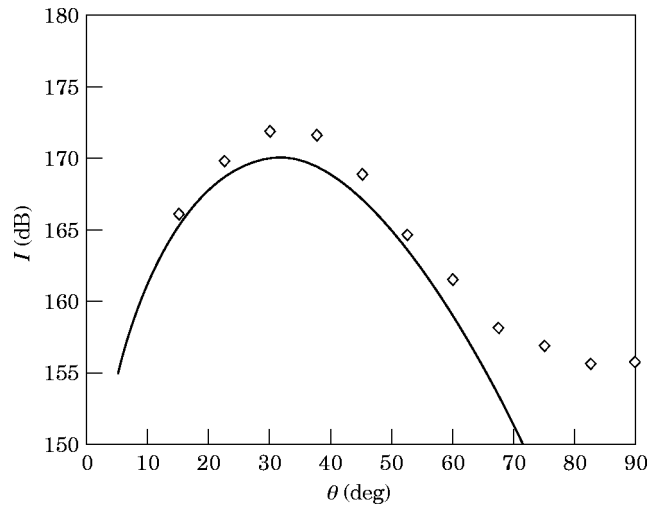


Figure 13. Jet at $M = 1.67$ and $T_j/T_0 = 1$. Acoustic directivity. —, Calculated; ◇, measurements of Tanna *et al.* [9] for a jet at $M = 1.65$.

TABLE 2

Acoustic field radiated by a free turbulent flow: dimensional laws

Convection Mach number	Subsonic	Supersonic
Dimensional law	$W \sim \frac{\rho_l^2}{\rho_0} D^2 \frac{U_j^8}{c_0^5} \frac{1 + M_c^2}{(1 - M_c^2)^4}$	$W \sim \frac{\rho_l^2}{\rho_0} D^2 U_j^3$
Efficiency	$\eta \sim \frac{\rho_l}{\rho_0} \left(\frac{U_j}{c_0} \right)^5 \frac{1 + M_c^2}{(1 - M_c^2)^4}$	$\eta \sim \frac{\rho_l}{\rho_0}$

4.2.2. Narrow band acoustic spectra

Narrow band power spectral densities provide further information on the radiated acoustic field. The power spectral density model developed in section 3 is now used to predict narrow band spectra. Figures 14 and 15 display the Mach wave noise directivity for a set of Strouhal numbers for cold and hot jets at $M = 2$. The predicted directivities are compared on one hand with measurements of Seiner *et al.* [3], and on the other hand, for the first case, with numerical results of Tam and Chen [1] obtained from an instability wave model (see section 2). The Strouhal number or dimensionless frequency St is defined in terms of the nozzle diameter D and the nominal velocity of the jet U_j : $St = fD/U_j$. It appears that the peak directivity data increases with the Strouhal number. This behaviour is associated with refraction effects which become more important as frequency increases. The predicted results feature this shift, in particular for the case $M = 2$ and $T_j/T_0 = 2.5$, where the curves follow the data points very closely. All the spectral directivity is not retrieved since only the Mach wave noise component is calculated. For the case $M = 2$ and $T_j/T_0 = 1$, the Tam and Chen calculations are plotted as a dashed line in Figure 14.

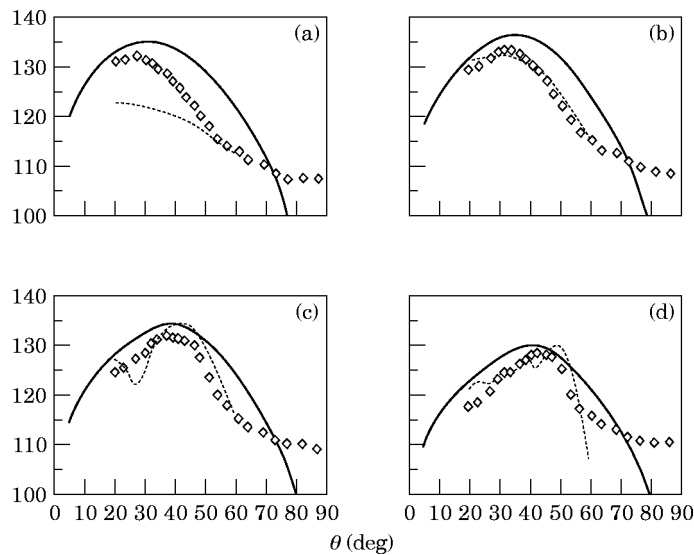


Figure 14. Directivity of Mach wave noise in dB, $M = 2.0$, and $T_j/T_0 = 1.0$ (a) $St = 0.067$; (b) $St = 0.12$, (c) $St = 0.20$, (d) $St = 0.40$. \diamond , Experimental data of Seiner *et al.* [3]. ---, Tam and Chen calculations [1].

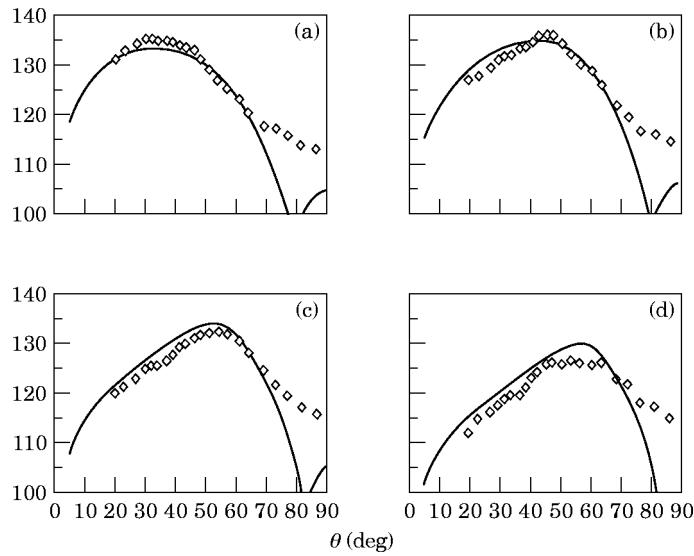


Figure 15. Directivity of Mach wave noise in dB, $M = 2.0$, and $T_j/T_0 = 2.5$ (a) $St = 0.05$; (b) $St = 0.10$, (c) $St = 0.20$, (d) $St = 0.40$. \diamond , Experimental data of Seiner *et al.* [3].

These results feature the directivity around the Mach wave angle except for the first Strouhal number $St = 0.067$. For this same case, our model overestimates the measurements by about 3 dB. Examination of these two jet configurations shows that our model correctly predicts the spectral directivity.

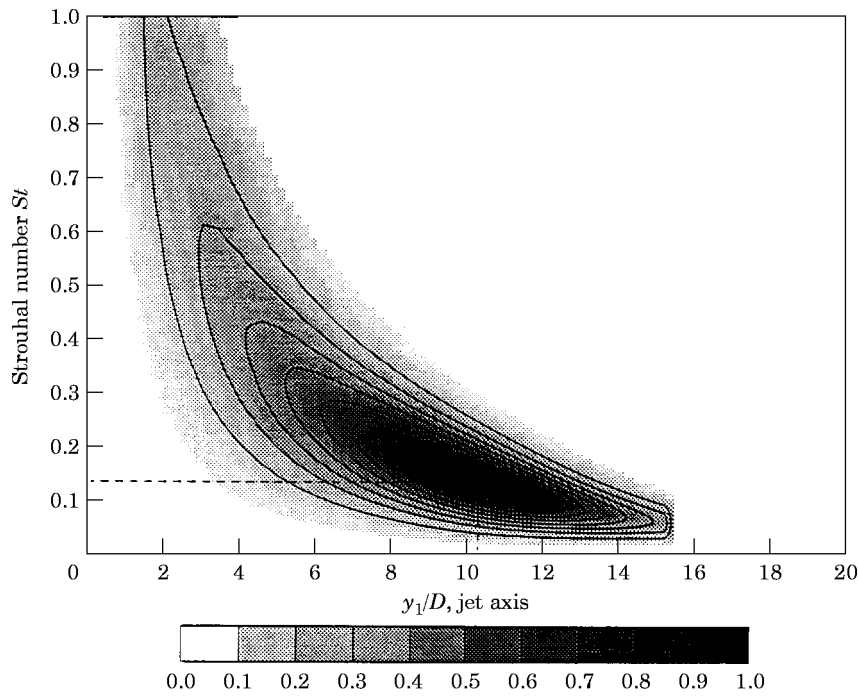


Figure 16. Equal contours of the normalized acoustic power spectral density per unit length. $\theta = 3^\circ$, $M = 2.0$ and $T_j/T_0 = 1.0$.

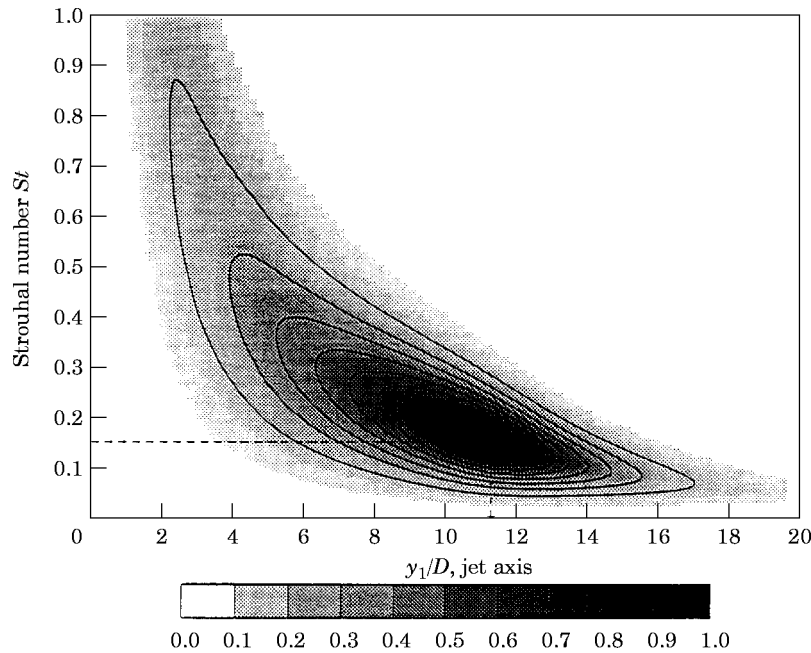


Figure 17. Equal contours of the normalized acoustic power spectral density per unit length. $\theta = 51^\circ$, $M = 2.0$ and $T_j/T_0 = 2.5$.

4.2.3. Distribution of the axial power spectral density

To complete the description of the acoustic radiation, an analysis of the power spectral density per unit length along the jet axis is displayed in Figures 16 and 17, for the two jets at $M = 2$. For the peak directivity angle θ^* of Mach waves, the power spectral density integrated over the jet cross section is plotted as a function of the Strouhal number St . The high frequency sources are located in the mixing region near the nozzle while the low frequency sources are situated in the downstream region, near the tip of the potential core. The space-frequency distribution of acoustic sources are similar to those obtained for subsonic jets, see references [23, 24]. However the maximum y_1^*/D is located further downstream near $y_1^*/D \simeq 10$ for $M = 2$ and $T_j/T_0 = 1$, and near $y_1^*/D \simeq 7.2$ for $M = 0.86$; see Table 3. The maximum seems always situated at the end of the potential core which increases with the Mach number. This result is in agreement with earlier experimental work of Laufer *et al.* [35].

Figure 18 displays predicted angular dependence of the peak spectral amplitude and measurements of Seiner *et al.* [3] in the case of a $M = 2$ and $T_j/T_0 = 2.5$ jet. The predicted peak spectral amplitude is again close to the experimental data. But for small angles, the strong refraction effects due to the mean flow gradient are not taken into account in the model. As a consequence the predicted results do not decrease quite like the measurements.

TABLE 3
Localization of the apparent Mach wave sources

M	T_j/T_0	θ^*	y_1^*/D	St^*
2.0	1.0	39°	10.3	0.13
2.0	2.5	51°	11.3	0.15

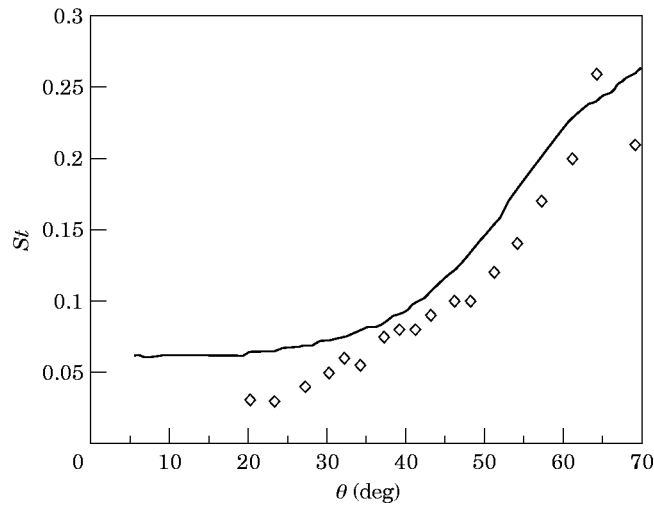


Figure 18. Angular dependence of the peak spectral amplitude, $M = 2.0$ and $T_j/T_0 = 2.5$. —, Calculated; \diamond , measurements of Seiner *et al.* [3].

Besides, the experimental data can be interpreted as follows. The power spectral density per unit length of the jet shows that the high frequency sources are located near the nozzle, where the convection Mach number M_c is highest. So, the corresponding Mach wave angle $\theta^* = \cos^{-1}(1/M_c)$ is larger than the one associated with the low frequency sources located downstream where the convection Mach number is smaller.

5. DISCUSSION AND CONCLUSION

A numerical procedure for calculating Mach wave noise has been described. The modelling of the source term relies on the work of Ffowcs Williams and Maidanik. From their analysis, an analytic formulation of the acoustic source term may be deduced for axisymmetric jets and an integral expression is finally derived from the power spectral density. One shows that the local knowledge of the mean flow and a characteristic time of turbulence allow an evaluation of the acoustic Mach wave noise radiation to be made. Aerodynamic calculations are carried out by using a $k-\epsilon$ turbulence code modified for compressible shear flows. Hence, this approach systematically employs local mean flow data for acoustic prediction. The model only requires a single unknown multiplicative constant. Cold jets at $M = 1.7$ and at $M = 2.0$ and a $M = 2.0$ hot jet ($T_j/T_0 = 2.5$) are investigated. Directivities are in good agreement with experimental data. Furthermore the spectral results obtained in the case of the hot jet are close to the measurements. These comparisons are encouraging: a complete picture of the space-frequency radiated acoustic field has been obtained. This method could be used to compare predicted space-frequency distributions of acoustic sources with those of modern imaging techniques applying to supersonic jets, or to study coaxial subsonic-supersonic jets. One notes that a similar approach has already been developed for subsonic and weakly supersonic jets. The case of a coaxial subsonic-subsonic streams has been treated with success in reference [25].

One original feature of the present study is that the calculation of Mach wave radiation is based on a CFD determination of the flow field. The method requires a $k-\epsilon$ turbulence code, a standard computational tool.

In a more general flow configuration, the present approach has two limitations. First, it requires a specific Green function for use in the integral formulation of Lighthill's

equation. Secondly, refraction effects due to mean flow gradients are not taken into account but they are known to modify the aerodynamic noise spectrum and directivity.

ACKNOWLEDGMENTS

This work has been supported by the Centre National d'Études Spatiales. Most of the simulations were carried out on a Cray C98 of the Institut du Développement et des Ressources en Informatique Scientifique to which the authors express their gratitude.

REFERENCES

1. C. K. W. TAM and P. CHEN 1993 *Proceedings of the 15th Aeroacoustic Conference, AIAA Paper* 93-4408, Long Beach, CA. Turbulent mixing noise from supersonic jets.
2. C. K. W. TAM 1995 *Annual Review of Fluid Mechanics* **27**, 17-43. Supersonic jet noise
3. J. M. SEINER, M. K. PONTON, B. J. JANSEN and N. T. LAGEN 1992 *Proceedings of the 14th Aeroacoustic Conference, AIAA Paper* 92-02-046, Eurogress Center Aachen. The effects of temperature on supersonic jet noise emission.
4. J. E. FFWCS WILLIAMS and G. MAIDANIK 1965 *Journal of Fluid Mechanics* **21**, 641-657. The Mach wave field radiated by supersonic turbulent shear flows.
5. A. L. KISTLER and W. S. CHEN 1962 *Journal of Fluid Mechanics* **16**, 41-64. The fluctuating pressure field in a supersonic turbulent boundary layer.
6. J. LAUFER 1962 *Centre National de la Recherche Scientifique, France, report* **108**. Sound radiation from a turbulent boundary layer.
7. S. P. PARTHASARATY and P. F. MASSIER 1976 *American Institute of Aeronautics and Astronautics Journal* **15**, 1462-1468. Mach wave emission from supersonic jets.
8. S. P. PARTHASARATY, P. F. MASSIER, R. F. CUFFEL and J. R. RADBILL 1976 *Progress in Astronautics and Aeronautics* **43**, 283-305. Density fluctuations and radiated noise for a high-temperature supersonic jet.
9. H. K. TANNA, P. D. DEAN and R. H. BURRIN 1976 *Air Force Aero-Propulsion Laboratory, Technical Report* 76-65. The generation and radiation of supersonic jet noise, Vol. III Turbulent mixing noise data.
10. H. K. TANNA 1977 *Journal of Sound and Vibration* **50**, 405-428. An experimental study of jet noise, Part I: turbulent mixing noise.
11. M. J. LIGHTHILL 1952 *Proceedings of the Royal Society of London* **A211**, 1107, 564-587. On sound generated aerodynamically-I. General theory.
12. M. J. LIGHTHILL 1954 *Proceedings of the Royal Society of London* **A222**, 1148, 1-32. On sound generated aerodynamically-II. Turbulence as a source of sound.
13. J. E. FFWCS WILLIAMS 1963 *Philosophical Transactions of Royal Society of London* **A255**, 469-503. The noise from turbulence convected at high speed.
14. M. E. GOLDSTEIN 1976 *Aeroacoustics*. New York: McGraw-Hill.
15. H. S. RIBNER 1964 in *Advances in Applied Mechanics (New York: Academic Press)* **VIII**, 103-182. The generation of sound by turbulent jets.
16. I. PROUDMAN 1952 *Proceedings of the Royal Society of London* **A214**, 119-132. The generation of sound by isotropic turbulence.
17. H. S. RIBNER 1969 *Journal of Fluid Mechanics* **38**, 1-24. Quadrupole correlations governing the pattern of jet noise.
18. S. P. PAO and M. V. LOWSON 1970 *Proceedings of the 8th Aerospace Sciences Meeting, AIAA Paper* 70-223, New York, N.Y. Some applications of jet noise theory.
19. M. E. GOLDSTEIN and B. ROSENBAUM 1973 *Journal of the Acoustical Society of America* **54**, 630-645. Effect of an isotropic turbulence on aerodynamic noise.
20. M. E. GOLDSTEIN and W. L. HOWES 1973 *National Aeronautics and Space Administration, Technical Note, D-7158*. New aspects of subsonic aerodynamic noise theory.
21. D. G. CRIGHTON 1975 *Progress in Aerospace Science* **16**, 31-96. Basic principles of aerodynamic noise generation.
22. C. BAILLY, W. BÉCHARA, P. LAFON and S. CANDEL 1993 *Proceedings of the 15th Aeroacoustics Conference, AIAA Paper* 93-4412 Long Beach, CA. Jet noise predictions using a $k-\epsilon$ turbulence model.

23. C. BAILLY 1994 *Ph.D. Thesis, Ecole Centrale Paris, 1994, France*. Modélisation du rayonnement acoustique des écoulements turbulents libres subsoniques et supersoniques.
24. C. BAILLY, P. LAFON and S. CANDEL 1994 *Acta Acustica* **2**, 101–112. Computation of subsonic and supersonic jet mixing noise using a modified $k-\epsilon$ turbulence model for compressible free shear flows.
25. W. BÉCHARA, P. LAFON, C. BAILLY and S. CANDEL 1995 *Journal of the Acoustic Society of America* **97**, 3518–3551. Application of a $k-\epsilon$ model to the prediction of noise for simple and coaxial free jets.
26. O. M. PHILLIPS 1960 *Journal of Fluid Mechanics* **9**, 1–28. On the generation of sound by supersonic turbulent shear layers.
27. R. MANI 1976 *Journal of Fluid Mechanics* **73**, 753–778. The influence of jet flow on jet noise. Part 1. The noise of unheated jets.
28. G. M. LILLEY 1972 *Air Force Aero Propulsion Laboratory, Technical Report 72-53*. The generation and radiation of supersonic jet noise. Vol. IV—Theory of turbulence generated jet noise, noise radiation from upstream sources, and combustion noise. Part II: Generation of sound in a mixing region.
29. DOAK, P. E. 1972 *Journal of Sound and Vibration* **25**, 263–335. Analysis of internally generated sound in continuous materials: 2. A critical review of the conceptual adequacy and physical scope of existing theories of aerodynamic noise, with special reference to supersonic jet noise.
30. J. C. LAU, P. J. MORRIS and M. J. FISHER 1979 *Journal of Fluid Mechanics* **93**, 1–27. Measurements in subsonic and supersonic free jets using a laser velocimeter.
31. M. SAMINY and G. S. ELLIOTT 1990 *American Institute of Aeronautics and Astronautics Journal* **28**, 439–445. Effects of compressibility on the characteristics of free shear layers.
32. S. C. CROW 1970 *Studies in Applied Mathematics* **49**, 21–43. Aerodynamic sound emission as a singular perturbation problem.
33. J. E. FFWCS WILLIAMS 1974 *Journal of Fluid Mechanics* **66**, 791–816. Sound production at the edge of a steady flow.
34. J. M. SEINER, D. K. MCLAUGHLIN and C. H. LIU 1982 *National Aeronautics and Space Administration, Technical paper 2072*. Supersonic jet noise generated by large scale instabilities.
35. J. LAUFER, R. SCHLINKER and R. E. KAPLAN 1976 *American Institute of Aeronautics and Astronautics Journal* **14**, 489–497. Experiments on supersonic jet noise.
36. O. ZEMAN 1990 *The Physics of Fluids A* **2**, 178–188. Dilatation-dissipation: the concept and application in modelling compressible mixing layers.
37. A. J. FAVRE, J. J. GAVIGLIO and R. J. DUMAS 1958 *Journal of Fluid Mechanics* **3**, 344–356. Further space-time correlations of velocity in a turbulent boundary layer.
38. W. P. JONES 1979 in *Von Karman Institute for Fluid Dynamics, Lecture series 1979-2*. Prediction methods for turbulent flows.
39. B. E. LAUNDER and D. B. SPALDING 1974 *Computer Methods in Applied Mechanics and Engineering* **3**, 269–289. The numerical computation of turbulent flows.
40. A. J. CHORIN 1967 *Journal of Computational Physics* **2**, 12–26. A numerical method for solving incompressible viscous flow problems.
41. R. TEMAM 1969 *Archive for Rational Mechanics and Analysis* **32**, 135–153. On an approximate solution of the Navier-Stokes equations by the method of fractional steps: Part I.

APPENDIX A: EXPRESSION OF THE CORRELATION FUNCTION OF THE PRESSURE TIME DERIVATIVE

For a stationary process, where τ designates the time separation between the two times, $t' = t + \tau$:

$$\begin{aligned}
 \overline{\frac{\partial p}{\partial t}(\mathbf{x}, t) \frac{\partial p}{\partial t'}(\mathbf{x}, t')} &= \lim_{T \rightarrow \infty} \frac{1}{2T} \int_{-T}^{+T} \frac{\partial p}{\partial t}(\mathbf{x}, t) \frac{\partial p}{\partial t'}(\mathbf{x}, t') dt \\
 &= \lim_{T \rightarrow \infty} \frac{1}{2T} \int_{-T}^{+T} \frac{\partial p}{\partial t}(\mathbf{x}, t) \frac{\partial p}{\partial \tau}(\mathbf{x}, t) dt \\
 &= \lim_{T \rightarrow \infty} \frac{1}{2T} \frac{\partial}{\partial \tau} \int_{-T}^{+T} \frac{\partial p}{\partial t}(\mathbf{x}, t) p' dt.
 \end{aligned}$$

Upon integrating by parts, and remembering that stationary functions remain bounded, it follows that

$$\begin{aligned} \overline{\frac{\partial p}{\partial t}(\mathbf{x}, t) \frac{\partial p}{\partial t'}(\mathbf{x}, t')} &= \lim_{T \rightarrow \infty} \frac{1}{2T} \frac{\partial}{\partial \tau} \left\{ [pp'] - \int_{-T}^{+T} p \frac{\partial p'}{\partial t} dt \right\} \\ &= - \lim_{T \rightarrow \infty} \frac{1}{2T} \frac{\partial^2}{\partial \tau^2} \int_{-T}^{+T} pp' dt. \end{aligned}$$

Hence, the correlation function of the pressure time derivative can be expressed as

$$\overline{\frac{\partial p}{\partial t}(\mathbf{x}, t) \frac{\partial p}{\partial t'}(\mathbf{x}, t')} = - \frac{\partial^2}{\partial \tau^2} \overline{[pp']}, \quad t' = t + \tau. \quad (31)$$

APPENDIX B: SOME PROPERTIES OF THE FUNCTION g

A suitable form for the function g can be

$$g(\tau) = (1 - \alpha \omega_i^2 \tau^2) \exp(-\omega_i^2 \tau^2). \quad (32)$$

This function reaches a minimum for $\tau^* = (\alpha + 1)/\alpha \omega_i^2$, and then the function g takes the value $g(\tau^*) = -\alpha \exp\{-\alpha(\alpha + 1)/\alpha\}$.

According to experimental data of Parthasarathy *et al.* [7, 8], an acceptable choice for α is $\alpha = 5/4$ which leads to $g(\tau^*) \simeq -0.21$. Moreover, one needs the second derivative of the function g at $\tau = 0$: $d^2g/d\tau^2|_{\tau=0} = -2(\alpha + 1)\omega_i^2$.

To calculate the power spectral density (5) one needs the Fourier transform of g :

$$\begin{aligned} G(\omega) &= \frac{1}{2\pi} \int_{-\infty}^{+\infty} (1 - \alpha \omega_i^2 \tau^2) e^{-\omega_i^2 \tau^2} e^{i\omega \tau} d\omega \\ &= \frac{1}{2\pi} \int_{-\infty}^{+\infty} (1 - \alpha \omega_i^2 \tau^2) e^{-\omega_i^2 \tau^2} \cos(\omega \tau) d\omega \end{aligned}$$

A double integration by parts leads to

$$G(\omega) = \left[1 - \frac{5}{8} \left(1 - \frac{\omega^2}{2\omega_i^2} \right) \right] \frac{1}{2\sqrt{\pi}\omega_i} \exp\left[-\frac{\omega^2}{4\omega_i^2} \right].$$

APPENDIX C: TURBULENCE MODEL EQUATIONS AND THEIR NUMERICAL SOLUTION

The basic mean flow equations which are solved numerically are given in the following section. The modified $k-\epsilon$ turbulence model for compressible mixing layers is then described. The ESTET code is briefly presented in the final subsection.

C.1. MEAN FLOW EQUATIONS

A density-weighted (Favre [37]) average is often used for compressible flows. With this averaging procedure, the conservation equations of mass, momentum and energy are similar to those derived from the incompressible flows. Using the Favre average for each

variable $\phi = \tilde{\phi} + \phi'' = \overline{\rho\phi}/\bar{\rho} + \phi''$, except for the density ρ and the pressure p , one may write the mean flow equations as follows: (i) continuity equation

$$\partial\bar{\rho}/\partial t + \partial(\bar{\rho}\tilde{u}_i)/\partial x_i = 0;$$

(ii) momentum conservation equation,

$$\bar{\rho}(\partial\tilde{u}_i/\partial t + \tilde{u}_j\partial\tilde{u}_i/\partial x_j) = -\partial\bar{p}/\partial x_i + (\partial/\partial x_j)(\overline{\tau_{ij}} - \overline{\rho u_i'' u_j''}),$$

where $-\overline{\rho u_i'' u_j''}$ is the Reynolds stress tensor and τ_{ij} is the viscous stress tensor, which takes the following form for a compressible Newtonian fluid:

$$\tau_{ij} = \mu \left(\frac{\partial u_i}{\partial x_j} + \frac{\partial u_j}{\partial x_i} \right) - \frac{2}{3} \mu \frac{\partial u_k}{\partial x_k} \delta_{ij}, \quad \overline{\tau_{ij}} \approx \mu \left(\frac{\partial \tilde{u}_i}{\partial x_j} + \frac{\partial \tilde{u}_j}{\partial x_i} \right) - \frac{2}{3} \mu \frac{\partial \tilde{u}_k}{\partial x_k} \delta_{ij};$$

(iii) specific enthalpy conservation equation,

$$\bar{\rho} \left(\frac{\partial \tilde{h}}{\partial t} + \tilde{u}_j \frac{\partial \tilde{h}}{\partial x_j} \right) = \frac{\partial}{\partial x_j} \left(\frac{\lambda}{c_p} \frac{\partial \tilde{h}}{\partial x_j} - \overline{\rho u_j'' h''} \right) + \frac{\partial \bar{p}}{\partial t} + \tilde{u}_j \frac{\partial \bar{p}}{\partial x_j} + \left\{ \overline{\tilde{u}_j \frac{\partial \bar{p}}{\partial x_j}} + \overline{u_j'' \frac{\partial \bar{p}}{\partial x_j}} + \bar{\Phi} \right\},$$

where λ is the heat conductivity, c_p the specific heat at constant pressure and Φ the viscous dissipation function, $\Phi = \tau_{ij} \partial u_i / \partial x_j$. One assumes a Fourier law for the heat flux vector $\mathbf{q} = -\lambda \nabla T$ and a perfect gas behaviour $dh = c_p dT$. The term $\overline{\rho u_j'' h''}$ is modelled by means of a gradient closure: $-\overline{\rho u_j'' h''} \approx (\mu_t / \sigma_t) \partial \tilde{h} / \partial x_j$.

In this expression μ_t is the turbulent viscosity and σ_t is the turbulent Prandtl number. The three last terms of the enthalpy equation (in brackets) are neglected in the numerical solution.

C.2. TURBULENCE MODEL

A modified $k-\epsilon$ turbulence model for compressible mixing layers is used to calculate the Reynolds stresses. The modification concerns the dissipation ϵ and is based on works of Zeman [36]. In this section, only the final form of the $k-\epsilon$ turbulence model is presented. The kinetic energy k and the dissipation rate ϵ are given by

$$k = \frac{1}{2} = \overline{u_i'' u_i''} = \frac{1}{2} \frac{\overline{\rho u_i'' u_i''}}{\bar{\rho}}, \quad \epsilon = \frac{1}{\bar{\rho}} \overline{\tau_{ij}'' \frac{\partial u_i''}{\partial x_j}}.$$

The dissipation ϵ of this kinetic energy is the sum of two contributions $\epsilon = \epsilon_s + \epsilon_d$ where ϵ_s is the solenoidal dissipation associated with the incompressible part of the velocity field. The distribution of this dissipation is given by the standard transport equation for the dissipation. The dilatation dissipation ϵ_d resulting from dilatation effects of the velocity field is given by the following expression proposed by Zeman:

$$\epsilon = \epsilon_s + \epsilon_d = \epsilon_s [1 + c_d f(M_t)] \text{ with } M_t = \sqrt{2k}/c \text{ and } c_d = 0.75.$$

Here the function f is given by

$$\left\{ \begin{array}{ll} f(M_t) = 1 - \exp \left[- \left(\frac{M_t - 0.1}{0.6} \right)^2 \right] & \text{if } M_t > 0.1 \\ f(M_t) = 0 & \text{if } M_t \leq 0.1 \end{array} \right\}.$$

The transport equations for k and ϵ take the following forms:

$$\bar{\rho} \left(\frac{\partial k}{\partial t} + \tilde{u}_j \frac{\partial k}{\partial x_j} \right) = \frac{\partial}{\partial x_j} \left[\left(\mu + \frac{\mu_t}{\sigma_k} \right) \frac{\partial k}{\partial x_j} \right] + \mathbf{P} + \mathbf{G} - \bar{\rho} \epsilon,$$

$$\bar{\rho} \left(\frac{\partial \epsilon_s}{\partial t} + \tilde{u}_j \frac{\partial \epsilon_s}{\partial x_j} \right) = \frac{\partial}{\partial x_j} \left[\left(\mu + \frac{\mu_t}{\sigma_\epsilon} \right) \frac{\partial \epsilon_s}{\partial x_j} \right] + \frac{\epsilon_s}{k} [C_{e1}(\mathbf{P} + \mathbf{G}) - C_{e2} \bar{\rho} \epsilon_s].$$

By using the eddy viscosity concept, which relates the Reynolds stresses to the mean flow gradients, the production term \mathbf{P} may be written as

$$\mathbf{P} = -\overline{\rho u_i'' u_j''} \frac{\partial \tilde{u}_i}{\partial x_j} = \left[\mu_t \left(\frac{\partial \tilde{u}_i}{\partial x_j} + \frac{\partial \tilde{u}_j}{\partial x_i} - \frac{2}{3} \frac{\partial \tilde{u}_k}{\partial x_k} \delta_{ij} \right) - \frac{2}{3} \bar{\rho} k \delta_{ij} \right] \frac{\partial \tilde{u}_i}{\partial x_j},$$

where μ_t is the turbulent viscosity given by $\mu_t = \bar{\rho} C_\mu k^2 / \epsilon_s$. The other production term \mathbf{G} is calculated by Jones [38] as

$$\mathbf{G} = \frac{\overline{\rho' u_i''}}{\bar{\rho}} \frac{\partial \bar{p}}{\partial x_i} = -\frac{1}{\bar{\rho}} \frac{\mu_t}{\sigma_t} \frac{\partial \bar{p}}{\partial x_i} \frac{\partial \bar{p}}{\partial x_i} \text{ with } 0.7 \leq \sigma_t \leq 1.$$

Standard values of the empirical constants of the k — ϵ model given by Launder and Spalding [39] are used in the calculations: $C_\mu = 0.09$ $C_{e1} = 1.44$ $C_{e2} = 1.92$ $\sigma_k = 1.0$ $\sigma_\epsilon = 1.3$

C.3. THE ESTET CODE

The ESTET code has been developed by the Laboratoire National Hydraulique of the Direction des Etudes et Recherches d'Electricité de France. The algorithm is based on the projection method, introduced by Chorin [40] and Temam [41], for the time discretization of the Navier-Stokes equations. A characteristic method is used for the convection step. The diffusion step and the pressure-continuity step (or projection step) are solved using implicit methods. The mesh is structured but irregular and all the calculations are performed with an axisymmetric version of ESTET.